NASA TECHNICAL NOTE

NASA TN D-7711

NASA TN D-7711



# A NEW APPROACH TO MASS SPECTROMETER MEASUREMENTS OF THERMOSPHERIC DENSITY

*by Leonard T. Melfi, Jr., F. J. Brock, and Clarence A. Brown, Jr.*

*Langley Research Center*
*Hampton, Va. 23665*

NATIONAL AERONAUTICS AND SPACE ADMINISTRATION • WASHINGTON, D. C. • SEPTEMBER 1974

| 1. Report No. NASA TN D-7711 | 2. Government Accession No. | 3. Recipient's Catalog No. |
|---|---|---|
| 4. Title and Subtitle<br>A NEW APPROACH TO MASS SPECTROMETER MEASUREMENTS OF THERMOSPHERIC DENSITY | | 5. Report Date<br>September 1974<br>6. Performing Organization Code |
| 7. Author(s)<br>Leonard T. Melfi, Jr., F. J. Brock, and Clarence A. Brown, Jr. | | 8. Performing Organization Report No.<br>L-9553<br>10. Work Unit No.<br>188-36-56-03 |
| 9. Performing Organization Name and Address<br>NASA Langley Research Center<br>Hampton, Va. 23665 | | 11. Contract or Grant No.<br>13. Type of Report and Period Covered<br>Technical Note |
| 12. Sponsoring Agency Name and Address<br>National Aeronautics and Space Administration<br>Washington, D.C. 20546 | | 14. Sponsoring Agency Code |

15. Supplementary Notes

Part of this work has been previously published in Review of Scientific Instruments, volume 44, no. 10, October 1973.

F. J. Brock is a Research Professor, Dept. of Physics, Old Dominion University, Norfolk, Va.

16. Abstract

The gas sampling problem in satellite and high-velocity probes has been investigated by applying the theory of a drifting Maxwellian gas. A lens system using a free-stream ion source has been developed and experimentally evaluated over the pressure range $10^{-5}$ to $10^{-2}$ N/m$^2$ ($\approx 10^{-7}$ to $10^{-4}$ torr). The source has high beam transparency, which minimizes gas-surface collisions within or near the ionization volume. It has been shown for high ion energy (60 eV) that the extracted ion beam has an on-axis energy spread of less than 4 eV and that 90 percent of the ions are within $2.5^{\circ}$ of the beam axis. From these studies, it is concluded that the molecular beam mass spectrometer concept developed for gas density measurements in the upper atmosphere substantially reduces gas-surface scattering and gas-surface reactions in the sample and preserves the integrity of the gas sample during the analysis process. Studies have shown that both the Scout and Delta vehicles have adequate volume, control, velocity, and data acquisition capability for obtaining thermospheric number density in real time.

| 17. Key Words (Suggested by Author(s)) | 18. Distribution Statement |
|---|---|
| Mass spectrometer<br>Molecular beam<br>Thermospheric measurements | Unclassified – Unlimited<br>STAR Category 13 |

| 19. Security Classif. (of this report) | 20. Security Classif. (of this page) | 21. No. of Pages | 22. Price* |
|---|---|---|---|
| Unclassified | Unclassified | 32 | $3.25 |

*For sale by the National Technical Information Service, Springfield, Virginia 22151

# A NEW APPROACH TO MASS SPECTROMETER MEASUREMENTS OF THERMOSPHERIC DENSITY*

By Leonard T. Melfi, Jr., F. J. Brock,**
and Clarence A. Brown, Jr.
Langley Research Center

## SUMMARY

The gas sampling problem in satellite and high-velocity probes has been investigated by applying the theory of a drifting Maxwellian gas. A lens system using a free-stream ion source has been developed and experimentally evaluated over the pressure range $10^{-5}$ to $10^{-2}$ N/m$^2$ ($\approx 10^{-7}$ to $10^{-4}$ torr). The source has high beam transparency, which minimizes gas-surface collisions within or near the ionization volume. It has been shown for high ion energy (60 eV) that the extracted ion beam has an on-axis energy spread of less than 4 eV and that 90 percent of the ions are within $2.5^{\circ}$ of the beam axis. From these studies, it is concluded that the molecular beam mass spectrometer concept developed for gas density measurements in the upper atmosphere substantially reduces gas-surface scattering and gas-surface reactions in the sample and preserves the integrity of the gas sample during the analysis process. Studies have shown that both the Scout and Delta vehicles have adequate volume, control, velocity, and data acquisition capability for obtaining thermospheric number density in real time.

## INTRODUCTION

Mass spectrometer experiments (refs. 1 to 3) have been performed to determine the structure of the terrestrial thermosphere (>80 km) for the past two decades. Complex data reduction schemes (ref. 4) to eliminate kinematic effects are required to interpret the data from these experiments. These schemes contain unsubstantiated simplifying assumptions and require the unknown atmospheric temperature as an input. Further, the adsorption and recombination of chemically active gases, such as atomic oxygen – a principal thermospheric constituent – on the surfaces of the instrument before ionization causes large errors in density measurements of this constituent. Theoretical studies (ref. 5) indicate that all previously published data on oxygen number density should be

---

*Part of this work has been previously published in Rev. Sci. Instrum., vol. 44, no. 10, Oct. 1973.

**Research Professor, Department of Physics, Old Dominion University, Norfolk, Va.

considered a lower limit, since they could be in error by as much as a factor of 4. Preliminary results (ref. 6) from an experiment in which the walls of the ion source of the mass spectrometer (ref. 7) were cooled to temperatures near that of liquid helium have confirmed these studies. Since 1967, attempts have been made (ref. 8) to account for the gas-surface effect in the measurements of oxygen density and have met with limited success.

This paper discusses a new measurement technique which does not require cryogenic cooling, substantially reduces gas-surface scattering and surface reaction, minimizes kinematic effects, and is also independent of gas temperature. The mass spectrometer system uses a free-stream (high-transparency) ion source mounted on a truncated cone and a molecular beam formed by the high velocity of the vehicle to effect the measurement. This technique may be used to perform experiments carried by rocket or entry probes into a planetary atmosphere, where measurements are required down to low altitude (<100 km in the terrestrial atmosphere), and satellite-borne experiments intended to characterize the upper atmosphere accurately.

The kinetic theory of a drifting Maxwellian gas has been used to show that gas-surface scattering may be reduced to an insignificant level. A hot-cathode ion source with high beam transparency has been developed, and the energy and angular distributions of the extracted ion beam have been experimentally determined for a number of source electrostatic configurations. Studies have shown that the technique is suitable for thermospheric flight experiments aboard the Scout or Delta vehicle.

## SYMBOLS

| | |
|---|---|
| $d$ | spacing between retarder and suppressor grids, m |
| $\overline{E}$ | average ion energy, eV |
| $\Delta E$ | ion-energy spread (full width at half-maximum (FWHM)), eV |
| $F(S,\alpha,\Theta)$ | mean molecular flux density (see eq. (2)), molecules/$cm^2$-sec |
| $f(\vec{v})$ | Maxwellian distribution function, $(cm/sec)^{-3}$ |
| $i^+$ | ion current at Faraday collector, A |
| $i^-$ | total electron current, $i^- = i_e^- + i_g^-$, A |

| | |
|---|---|
| $i_e^-$ | electron current at extractor, A |
| $i_g^-$ | electron current at grid, A |
| K | ion-source constant, $K = \frac{i^+}{i^- p}$, $(N/m^2)^{-1}$ |
| k | Boltzmann constant, J/molecule-K |
| m | molecular weight, amu |
| n | molecular number density, molecules/$cm^3$ |
| p | pressure, $N/m^2$ |
| r | retarder mesh radius, m |
| S | speed ratio, $S = \frac{u}{v_m}$ |
| T | molecular temperature, K |
| $T_e$ | exospheric temperature, K |
| $\vec{u}$ | instrument velocity, m/sec |
| $V_d$ | deflector potential, V |
| $V_e$ | ion extractor potential, V |
| $V_f$ | lens grid potential, V |
| $V_g$ | electron collector (grid) potential, V |
| $V_k$ | cathode potential, V |
| $V_r$ | ion retarder potential, V |
| $V_s$ | electron suppressor potential, V |

$\vec{v}$ average molecular velocity, m/sec

$\bar{v}$ average thermal speed, m/sec

$v_m$ mean molecular speed, m/sec

$\vec{w}$ molecular velocity relative to instrument, $\vec{w} = \vec{v} + \vec{u}$, m/sec

$w,\theta,\phi$ drifting spherical coordinate system

$\alpha$ angle of attack (angle between instrument axis and vehicle velocity vector), deg

$\Theta$ plane half-angle which defines conical solid angle, deg

$\Psi$ angle between ion-beam axis and analyzer axis, deg

Subscripts:

x,y,z vector components

## MEASUREMENT PHILOSOPHY

In making in situ measurements of the composition of a planetary atmosphere, it is obviously desirable to obtain an unaltered sample of the gas and to maintain the integrity of this sample during the measurement. The sample must not interact with the measuring system and there must be no reactions among the sample constituents. From the kinetic theory of a drifting Maxwellian gas, it can be concluded that only the gas in a narrow forward-facing cone can reach the instrument if the instrument carrier speed is much greater than the mean thermal speed of the gas (assuming the local wind velocity is negligible compared with the vehicle velocity). A sample of the atmosphere can be obtained and measured by continuously passing this stream through a highly transparent ionization volume where a fraction of the gas is ionized, focused into an analyzer, and counted; the unused part of the stream can be returned to the free atmosphere with a very low probability that the molecules will scatter back into the ionization volume. There are available several attitude-controlled rocket systems which have sufficiently high speeds to make this technique practicable for measurements in the upper atmosphere of the Earth and other planets.

## KINETIC THEORY

The combined constraints on gas temperature, instrument velocity, and geometry can be obtained directly from the kinetic theory of a drifting Maxwellian gas. The mean molecular flux density incident on an incremental surface moving with a velocity $\vec{u}$ through a Maxwellian gas is given by

$$F(\vec{u}) = \int_{-u_Z}^{\infty} \int_{-\infty}^{\infty} \int_{-\infty}^{\infty} n(v_Z + u_Z)\, f(\vec{v}) dv_X dv_Y dv_Z \tag{1}$$

where the surface normal is parallel to the z-direction, $n$ is the molecular number density, $f(\vec{v}) = \pi^{-3/2} v_m^{-3} \exp\left[-\left(v_X^2 + v_Y^2 + v_Z^2\right)/v_m^2\right]$ is the Maxwellian distribution function, and $v_m = (2kT/m)^{1/2}$. When the transformation to a coordinate system which is fixed with respect to the surface (fig. 1) is made, the gas is transformed to a drifting Maxwellian gas and the relative molecular velocity is given by $\vec{w} = \vec{u} + \vec{v}$. Suppose that $w_Z$ is parallel to the surface normal, that $\vec{u}$ lies in the $w_Y, w_Z$ plane, and that $\alpha$ is the angle between $w_Z$ and $\vec{u}$. Upon transforming to spherical coordinates in w-space and performing all elementary integrations, the mean molecular flux density incident on the surface from within a prescribed conical solid angle defined by the plane half-angle $\Theta$ measured from $w_Z$ is given by

$$F(S,\alpha,\Theta) = \frac{n v_m \exp\left(-S^2\right)}{\sqrt{\pi}} \left\{ \frac{\sin^2 \Theta}{2} + \frac{S^2 \sin^2 \alpha \sin^4 \Theta}{8} + \frac{S^2 \cos^2 \alpha \left(1 - \cos^4 \Theta\right)}{4} \right.$$

$$\left. + \frac{1}{\sqrt{\pi}} \int_0^{\Theta} \sin\theta \cos\theta \int_0^{\pi} SY \exp\left(S^2 Y^2\right) \left[1 + \operatorname{erf}(SY)\right] \left(\frac{3}{2} + S^2 Y^2\right) d\phi\, d\theta \right\} \tag{2}$$

where $Y = \sin\theta \cos\phi \sin\alpha + \cos\theta \cos\alpha$ and the speed ratio is

$$S = \frac{u}{v_m} \tag{3}$$

Integration over the complete w half-space gives

$$F(S,\alpha,\pi/2) = \frac{n\bar{v}}{4} \left\{ \exp\left(-S^2 \cos^2 \alpha\right) + \sqrt{\pi}\, S \cos\alpha \left[1 + \operatorname{erf}(S \cos\alpha)\right] \right\} \tag{4}$$

where

$$\bar{v} = \left(\frac{8kT}{\pi m}\right)^{1/2}$$

The fraction of the flux density arriving at the surface from within a prescribed solid angle defined by $\Theta$ is given by $F(S,\alpha,\Theta)/F(S,\alpha,\pi/2)$ from equations (2) and (4). This ratio was evaluated by using a fifth-order integration routine to perform the $\phi$ integration for 100 equal increments of $\theta$ in the range $0 \leqq \theta \leqq \pi/2$ and for prescribed values of $S$ and $\alpha$ within the ranges $0 \leqq S \leqq 10$ and $0 \leqq \alpha \leqq \pi/2$. The trapezoidal rule was used to perform the $\theta$ integration from 0 to $\Theta$. Some results of these calculations are presented in figure 2 for $\alpha = 0^{\circ}$ and $\alpha = 9^{\circ}$. It may be seen from figure 2(a) ($\alpha = 0^{\circ}$) for $S = 6$ that 98.5 percent of the flux density is within $\Theta = 20^{\circ}$. Thus, less than 1.5 percent of the gas entering the system collides with the internal surface if the internal half-angle of the instrument is greater than or equal to $20^{\circ}$. The fraction of gas colliding with the internal surface is smaller for gas entering a truncated cone than for gas entering a cone having an infinitesimal entrance aperture. Thus, applying these calculations to the actual hardware (truncated cone) overestimates the fraction of the gas which collides with the wall.

## EXPERIMENT DESIGN

Most hot-cathode ion sources in use with flight mass spectrometers are based on the design of Bleakney (ref. 9) and Nier (ref. 10). Sources of this type do not minimize gas-surface scattering. The technique of measuring number density with mass spectrometers in flight requires that the density in the ionization volume be substantially the same as the free-stream density and that gas-surface and gas-gas scattering be reduced to a negligible level so that no species present in the free stream is substantially reduced in the ionization volume and so that no spurious species, not present in the free stream, is introduced into the ionization volume.

The requirements of maintaining free-stream density and minimizing scattering in the ion source are satisfied by a small-angle cone constructed of high-transparency mesh ($\geqq 0.95$), the enclosed volume of which is the ionization volume. (See fig. 3.) At low free-stream density (applicable to most of the anticipated flight regime), multiple scattering may be neglected. Thus gas scattered from the external surface never enters the ionization volume for any gas-surface scattering law, provided that the external surface of the support structure is a smooth continuation of the ion-source grid structure. Even at a relatively high free-stream density, where the external mean free path is relatively small, molecules scattered off the external surface can enter the ionization volume only through an external gas-gas collision. In these multiple events the probability

that the molecule is scattered in the direction of the ionization volume is small. Further, considering the near-grazing angle of incidence and the high relative velocity, the molecules incident on the external surface are reflected in a near-specular direction, so that the gas-gas collisions tend to occur too far aft for gas to be scattered into the ionization volume (until the density becomes sufficiently high to cause an incipient shock).

The high-transparency requirement on the mesh used to form the ion-source grid is not the only constraint on the mesh. Since gas molecules incident on the edge of the mesh members can scatter into the ionization volume, it is necessary that the thickness-width ratio of the mesh members be small (assuming a rectangular cross section). This requirement is particularly important if some fraction of this incident flux is thermally accommodated to the surface before it is scattered into the ionization volume, since the accommodated flux makes a spurious contribution to the density in the ionization volume. The relative magnitude of the spurious density component is proportional to the product of the speed ratio ($5 \leqq S \leqq 15$) and the fraction of the accommodated flux.

The requirement of minimizing scattering off the support structure may be satisfied by making the internal cone angle equal to or greater than the angle containing a prescribed fraction of the incident flux (consistent with the level of precision desired in the experiment) for the maximum angle of attack and minimum speed ratio expected in flight. This condition assures that only a small fraction of the gas passing through the ion source can collide with the inner surface of the support structure and only a small fraction of this gas can backscatter into the ionization volume, since under these conditions (near-grazing incidence and high relative velocity) the gas-surface scattering is nearly specular (refs. 11 to 14). Thus, substantially all the gas passes through the exit aperture of the ion-source support cone into the wake.

The ions extracted from the ionization volume are focused by an electrostatic lens onto the quadrupole entrance aperture. In the process of ion-beam formation and extraction, the ions are accelerated to a velocity which is large (3 to 5 for atomic oxygen) compared with the thermal velocity of the neutral gas. This minimizes the dependence of the distribution of ion-beam current density on gas temperature and small variations in angle of attack. The lens is located inside the support cone and its angular aperture is sufficiently large to allow only a small fraction of the neutral beam to collide with its surfaces. The quadrupole entrance aperture is located sufficiently far downstream to provide adequate area to exhaust to the wake for the primary flux passing through the ion source. Only a small fraction of this neutral beam enters the quadrupole enclosure. Around the periphery of the entrance aperture and near the aft end of the quadrupole enclosure, a large conductance to the wake is provided to minimize gas loading in the quadrupole enclosure. In flight, gas passes through these conductances only in the exit

direction, since the magnitude of the speed ratio is such that gas cannot enter from the free stream (until the density becomes sufficiently high to cause an incipient shock).

The cathode is a wire ring with a small cross section surrounding the ion-source grid and is located slightly aft of the grid base to minimize the probability that gas scattered from the cathode may enter the ionization volume.

Several ion sources were constructed and their performance was evaluated under equilibrium gas conditions. Design details of the source and data on energy distribution and angular distribution of the extracted ion beam are presented in the next section. Mass resolution and sensitivity data (ref. 15) were also obtained on a flight quadrupole mass filter. Line widths less than 1 amu for masses less than 40 amu were obtained for ion energies of the order of 60 eV. The sensitivity, as determined by measurement of the $N_2^+$ beam transmitted through the quadrupole, was approximately $10^{-8}$ $\frac{A}{N/m^2}$ for an emission current 100 $\mu$A.

## ION-SOURCE DESIGN AND EVALUATION

It is important that the instrument system be relatively insensitive to the molecular-velocity distribution of the relatively high-temperature gas in the thermosphere and also to small deviations of the instrument axis with respect to the vehicle velocity vector within the dead band of the attitude control system. It is therefore necessary to extract the ions at a velocity sufficiently high to insure that in the worst case the resultant velocity vector (total of the neutral molecular velocity relative to the instrument plus the velocity resulting from extraction and focusing) remains within a prescribed cone centered on the instrument axis. Considering the gas temperature, vehicle velocity, and pointing error expected in flight, the energy of the ion beam must be of the order of 60 eV or greater (ref. 15). Thus, in addition to investigating the performance of the ion source, it is necessary to determine the properties of the extracted ion beam.

The apparatus for ion-beam analysis shown in figure 4 was designed for the investigation of the properties of the extracted ion beam. Before assembly, each metal element of this system was fired in a vacuum furnace at 1300 K and at a pressure below $10^{-4}$ $N/m^2$ to eliminate gas trapped in the metal bulk. The system is enclosed in a grounded metal cylinder to provide a field-free region between the ion source and the analyzers. The ion-source elements are mounted on flat plates which are separated by 1-mm-thick ceramic spacers. The source is contained in a cubical enclosure to prevent spurious ions from drifting into the analyzer. This source assembly may be rotated about a transverse axis which lies in the plane containing the ion-source exit aperture. The circular hot cathode is constructed of 0.125-mm-diameter tungsten wire and is thoria coated to lower the cathode work function. It is mounted on a split plate to which

the power leads are attached. The cathode mounting plane is located 1.52 mm from the base of the conical grid. The $15^{o}$ half-angle conical grid has a base 6.3 mm in diameter and is 6.3 mm long.

Since transparency is not an important parameter in equilibrium experiments, an available tungsten mesh (with a transparency greater than 80 percent) was used in the construction of the grid. The extractor aperture is 6.3 mm in diameter and has its center on the cone axis. This aperture is covered with mesh having a central hole 3.12 mm in diameter. The exit aperture is 13 mm square and is mounted on the cubical enclosure. Attached to the exit aperture is a cylindrical three-element gridded lens (symmetrical). The inside diameter of the two cylinders is 7.5 mm and the diameter of the grid aperture is 1 cm. The cylinder lengths are 1 cm. The lens grid is separated from each cylinder by 1-mm-thick ceramic spacers. The lens cylinders are grounded internally. At the end of the lens are located electrostatic deflector plates which are 1.25 cm square and oriented so that their surface normal is parallel to the rotation axis of the ion source. The separation of the deflectors is 1 cm.

The analyzer system consists of an entrance aperture, an ion retarder, an electron suppressor, and a Faraday cup ion collector. The entrance has a 1.25-mm-diameter aperture and is located 4 cm from the source exit. Since the electrode containing the entrance aperture is isolated, it can be used as a collector for the total ion current extracted from the source. The retarder has a 6.3-mm-diameter aperture and is used to retard those ions with energy less than that corresponding to the retarder voltage. The suppressor electrode has an aperture 1.5 mm in diameter and functions as a secondary electron suppressor with respect to the Faraday collector and also functions as a shield for the Faraday collector. The Faraday ion collector has a 3.75-mm-diameter aperture and a length-diameter ratio greater than 5. Each of these apertures is mounted coaxially and is covered with mesh.

The apparatus was mounted on a copper-sealed metal flange and the electrode leads were brought out by ceramic-metal feedthroughs. An absolute calibration system (ref. 16) was used to perform the ion-source evaluations. This system is pumped by ion pumps, whose pumping speed for molecular nitrogen is 500 liters/sec, in conjunction with titanium sublimation and liquid nitrogen cryopanels to produce an ultimate pressure below $3 \times 10^{-9}$ $N/m^2$ in the calibration chamber after bakeout (650 K). The total measurement uncertainty in pressure for the calibration range $\left(10^{-7} \text{ to } 10^{-2} \text{ N/m}^2\right)$ of the system is ±5.5 percent for molecular nitrogen (ref. 17).

The ion-source sensitivity was established by measuring the ion current at the Faraday collector $i^+$ as a function of the known equilibrium pressure over the range $10^{-5}$ to $10^{-2}$ $N/m^2$ for a number of extractor voltages $V_e$. The results of these calibrations for $V_g = 60$ V, $V_e = 0$, and $V_e = 60$ V are shown in figure 5. On the ordinate

is plotted the normalized-ion source constant, which is the ion current at the Faraday collector divided by the total electron current times the pressure:

$$K = \frac{i^+}{i^- p} \tag{5}$$

The lens grid potential $V_f$ was set at -46 V for $V_e = 0$ and at -57 V for $V_e = 60$ V to maximize the current density at the analyzer entrance aperture. (The lens cylinders were grounded internally.) This focus condition was independent of pressure over the pressure range of the investigation.

In one plane, the ion beam was centered on the analyzer aperture by the electrostatic deflector $(V_d = \pm 3$ V); in the plane orthogonal to this plane, by rotating the ion source. No adjustment of the ion-beam centering voltage was required during the remaining evaluations. On the basis of a comparison of several preliminary energy-distribution curves taken at different suppressor potentials, a value of $V_s$ of -15 V was used. At pressures below $10^{-3}$ N/m$^2$, the ion-source constant in terms of Faraday collector current is independent of pressure (fig. 5). At pressures above $10^{-3}$ N/m$^2$, it decreased with pressure because of charge transfer and ion-neutral scattering.

The emission current $i^-$ used in the calibration was established from figure 6, which shows curves of source constant as a function of emission current between 1 and 1000 $\mu$A for both extractor voltages. For $V_e > V_k$, electrons can be collected at the extractor. The emission current plotted in this figure is the sum of the electron currents collected at the grid $i_g^-$ and at the extractor $i_e^-$. The ratio of these two currents is, however, independent of both pressure and emission current. Above 100 $\mu$A for $V_e = 0$ and above 50 $\mu$A for $V_e = 60$ V, the source constant decreases with emission current; this decrease is caused by depression of the potential distribution by electronic space charge within the ionization volume. This conclusion is confirmed by the ion-energy distribution curves given in figure 7.

The data for the curves in figure 7 were taken in a manner similar to that for the curves on the far right side of figures 8(a) and (b) (discussed later in this section); indeed, curves B and D were taken from figures 8(a) and (b) for comparison. Data on average energy and energy spread for the curves in figure 7 are given in table I. These data show that for higher emission currents (A or C), the average energy is lower and the energy spread is higher than for lower emission currents (B or D), respectively, for both electrical configurations, as would be expected if electronic space charge depressed the potential distribution within the ionization volume. The source constant for $V_e = 60$ V (see fig. 6) begins to decrease at a lower emission current than for $V_e = 0$, since the extractor is immersed in the electronic space charge at $V_e = 60$ V but repels the electron cloud at $V_e = 0$. This conclusion is supported by the measured electron current collected by the extractor, which for $V_e = 60$ V is approximately equal to the electron

TABLE I.- PARAMETERS FOR THE RETARDER-POTENTIAL CURVES SHOWN IN FIGURE 7

| Parameter | Values for curve – | | | |
|---|---|---|---|---|
| | A | B | C | D |
| Ion extractor potential, $V_e$, V | 0 | 0 | 60 | 60 |
| Lens grid potential, $V_f$, V | -46 | -46 | -57 | -57 |
| Cathode potential, $V_k$, V | 0 | 0 | 0 | 0 |
| Electron collector (grid) potential, $V_g$, V | 60 | 60 | 60 | 60 |
| Deflector potential, $V_d$, V | ±3 | ±3 | ±3 | ±3 |
| Ion retarder potential, $V_r$, V | See abscissa of figure 7 | | | |
| Electron suppressor potential, $V_s$, V | -15 | -15 | -15 | -15 |
| Ion current at Faraday collector, $i^+$, A | See ordinate (normalized) of figure 7 | | | |
| Electron current at grid, $i_g^-$, μA | 250 | 10 | 125 | 5 |
| Electron current at extractor, $i_e^-$, μA | 0 | 0 | 125 | 5 |
| Pressure, p, $N/m^2$ | $4 \times 10^{-4}$ | $4 \times 10^{-4}$ | $4 \times 10^{-4}$ | $4 \times 10^{-4}$ |
| Average ion energy, $\overline{E}$, eV | 53.0 | 56.2 | 56.0 | 57.8 |
| Ion-energy spread (FWHM), ΔE, eV | 3.5 | 3.4 | 2.5 | 2.3 |

current at the grid, or $i_e^-/i_g^- = 1.0$. From the geometry and the potential configuration for $V_e = 60$ V, it is clear that the extraction probability is highest for ions formed in the neighborhood of the extractor grids, since in this configuration the exit aperture acts as an extractor. However, for $V_e = 0$, electrons are excluded from the neighborhood of the extractor and no ions are formed in this region, but in this configuration the extractor potential penetrates into the grid space, so that the extraction probability is high for ions formed in a large fraction of the grid space.

The radial distribution of the current density was determined by rotating the ion-source enclosure about an axis lying in the aperture plane while measuring the current at the Faraday collector. Several curves of ion current as a function of angular displacement of the ion beam with respect to the analyzer axis $\Psi$ were obtained for the range $-9^o \leq \Psi \leq 9^o$. These data have established radial symmetry.

Ion current was measured as a function of $\Psi$ for a number of extractor voltages. The results for two of these voltages, $V_e = 0$ and $V_e = 60$ V, are shown on the far left side of figures 8(a) and (b). For both extractor voltages the ion beam has a narrow angular spread, approximately $1^o$ for $V_e = 0$ and $1.2^o$ for $V_e = 60$ V (FWHM). The acceptance angle of the analyzer system is larger than the angle subtended by the lens grid as viewed from the analyzer entrance. Considering the angular resolution of the analyzer ($1.9^o$), the actual angular spread is less than that implied by these data.

The energy distribution of the ion beam was determined with a retarding potential analyzer. The retarding grid was made of high-transparency mesh. Only those ions with energies higher than that corresponding to the retarder potential can pass through to the ion collector. A sweep generator was used to change the voltage slowly of a programmable power supply connected to the retarding grid, and the output of the electrometer measuring the retarded current was plotted as a function of the retarder potential for a number of angular positions and extractor potentials. Shown on the far right side of figures 8(a) and (b) are typical results for a number of angles $\Psi$ at extractor potentials $V_e = 0$ and $V_e = 60$ V. From the relationship (ref. 18) $\Delta E/\overline{E} = r^2/(16d^2)$, the energy resolution of the analyzer was calculated as 1/256. In this relationship the mesh radius $r$ is 0.25 mm and the spacing between the retarder grid and the suppressor grid $d$ is 1 mm.

It can be seen from figures 8(a) and (b) that the on-axis ions have energies which correspond to the grid voltage with an energy spread of less than 1.9 eV for $V_e = 60$ V and 3.7 eV for $V_e = 0$. The lower energy spread for $V_e = 60$ V than for $V_e = 0$ implies a more uniform potential distribution within the ionization volume, as expected.

## FLIGHT DEMONSTRATION STUDIES

The feasibility of a flight demonstration of the experiment was examined after the instrument concept had been successfully demonstrated in the laboratory. Studies were made of satellite missions (both primary and piggyback experiments) and a suborbital reentry profile. A high-velocity vehicle is required to apply this mass spectrometer technique; thus it is well suited to satellite studies of the upper atmosphere.

### Primary Satellite Missions

Speed ratios for an orbital experiment would be approximately 10 for atomic oxygen and 5 for helium. With a cone internal half-angle of over 25°, even helium gas-surface collision at $\alpha = 0^\circ$ may be minimized. (See fig. 2.) Further, gas-gas scattering effects are negligible since satellite perigees are generally well above the altitude at which gas-gas scattering becomes important. Most large satellite payloads contain attitude control systems, the pointing accuracy of which exceeds the requirements of this technique. Even in many spin-stabilized satellites having no active attitude-control system, useful measurements may be made. As an example, at $\alpha = 9^\circ$ (see fig. 2), only 4 percent of the helium atoms would make wall collisions. The instrument can be mounted in the free stream with its axis orthogonal to the axis of rotation so that the instrument axis passes through ram each rotation. For spin rates less that 5 rpm, adequate time (>0.6 sec/mass scan) is available to measure each constituent.

## Piggyback Missions

Studies were conducted to determine whether piggyback experiments carried on several types of NASA launch vehicles, which traverse the lower thermosphere, would be feasible. These included (a) a suborbital ballistic trajectory flying on the third stage of a Scout vehicle, and (b) an orbital experiment aboard the terminal vehicle payload interstage of a Delta vehicle. Both the speed and the onboard orientation capabilities of these vehicles would satisfy the requirements for this technique. Further, the cost associated with such a piggyback demonstration would not be prohibitive. These two studies are discussed next.

Suborbital Scout mission.- If the suborbital reentry experiment were performed on the Scout vehicle (see fig. 9(a)), the atmospheric analysis system would be mounted on its third stage. (See fig. 9(b).) At initial perigee, this stage is used to aline the fourth stage, which injects the satellite into orbit. (See fig. 9(c).) The third stage then follows a ballistic trajectory from this altitude to impact. The onboard control system of this stage can be used to aline the instrument axis with the vehicle velocity vector over the altitude test interval from above 300 km to below 100 km in the terrestrial thermosphere.

A feasibility study for an early 1974 launch was made with the use of Jacchia's thermospheric temperature profiles (ref. 19). For these temperature data and the vehicle speed obtained from a typical third-stage ballistic trajectory, the speed ratio as a function of altitude for atomic oxygen was calculated and is shown in table II. The calculation was based on atomic oxygen, since it has the highest mean thermal velocity of the chemically active gases in the thermosphere. It can be seen from this table that below 300 km, $S$ exceeds 5.5 and, with an internal cone angle equal to $20^{\circ}$ or greater, the fraction of the gas which makes internal wall collisions is less than 0.02. (See fig. 2.) As previously mentioned, the application of the results of kinetic theory to the hardware must overestimate the fraction of the gas which has wall collisions, since the instrument entrance aperture is not infinitesimally small. Even with the most conservative reflection law (diffuse), only a small fraction of the surface-scattered gas can enter the ionization volume.

A more realistic law is specular scattering, since most of the molecules make collisions at near-grazing angles at high relative velocities. If the scattering is specular, substantially all of the gas will be scattered into the wake and cannot reach the ionization region. At lower altitudes, $S$ increases as a result of both the sharp decrease in gas temperature between 200 and 120 km and the increase in vehicle speed; thus, a completely negligible fraction of the primary beam is incident on the internal surface of the cone. The speed ratios for the Scout probe, given in table II, applied to the results from the kinetic theory confirm that an experiment with minimum gas-surface scattering effects could be performed in this altitude range. The low-altitude limit of the operating

TABLE II.- SPEED RATIO* AT A GIVEN ALTITUDE FOR ATOMIC OXYGEN FOR EXOSPHERIC TEMPERATURES $T_e$ OF 900 K AND 1000 K

[A typical Scout reentry probe]

| Altitude, km | Speed ratio for – | |
|---|---|---|
| | $T_e$ = 900 K | $T_e$ = 1000 K |
| 300 | 5.78 | 5.52 |
| 280 | 5.86 | 5.57 |
| 260 | 5.92 | 5.63 |
| 240 | 6.00 | 5.71 |
| 220 | 6.09 | 5.82 |
| 200 | 6.22 | 5.96 |
| 180 | 6.42 | 6.17 |
| 160 | 6.75 | 6.54 |
| 140 | 7.53 | 7.36 |
| 120 | 9.73 | 9.60 |
| 100 | 13.03 | 13.00 |
| 90 | 13.54 | 13.54 |

*See equation (3).

regime is determined by gas-gas scattering. As the mean free path inside the instrument becomes small, compared with the instrument dimensions, a nonnegligible fraction of the flux is accommodated to the wall temperature, and gas loading within the instrument occurs. Further, as the external free path decreases, the presence of an incipient shock probably alters the gas composition before it can be sampled. An analysis of gas-gas scattering indicates that measurements with the present technique may be made to below 100 km.

Orbital Delta mission.- To perform the orbital experiment on the Delta vehicle (fig. 10(a)), the mass spectrometer would be mounted on its second stage (fig. 10(b)). This guidance stage attains orbit and has restart capability. This capability allows orbital reshaping to bring perigee within the range of data-acquisition ground stations and to adjust the eccentricity so that the section of the atmosphere of most interest (i.e., orbit at 185 km to 463 km) is analyzed. Figure 10(c) shows a ground track of this orbit, including tracking stations and their altitude tracking range.

From these flight demonstration studies, it has been concluded that this instrument concept may be applied on primary satellite missions and in a piggyback mode on both the Scout and the Delta vehicles.

## CONCLUSIONS

The theory of a drifting Maxwellian gas has been applied to the development of a mass spectrometer technique which allows density measurements to be made in the upper atmosphere without the inaccuracies caused by gas-surface interactions. This technique employs a free-stream ion source and molecular beam technology. It has been shown that at high velocity (6 to 8 km/sec) a relatively narrow molecular beam is formed behind an aperture moving through the atmosphere. For atomic oxygen in the terrestrial atmosphere, 99 percent of the flux is contained within a beam divergence angle of less than $20^{\circ}$. It has been concluded from the theory that for a conical instrument geometry having a half-angle greater than $20^{\circ}$ moving through the atmosphere at high velocity, substantially no internal collisions occur and the constraint to minimize gas-surface collisions within the instrument is satisfied.

A further constraint is the beam transparency of the ion source. Since most ion sources are not transparent, one was developed which has a transparency of 95 percent to neutral gas molecules. It has been shown from the experimental evaluation of this source that it is acceptable for application to mass analyzers. The on-axis ion energy spread at 60 eV is less than 4 eV and 90 percent of the ions are contained within $2.5^{\circ}$ of the source axis.

A number of vehicle systems (including the Scout and Delta) have been studied and were found to be suitable for a meaningful thermospheric flight experiment. It has been concluded that on the Scout vehicle, in a suborbital mode, measurements of constituent density can be made over the altitude range between 300 and 100 km. Further, on the Delta vehicle, in an orbital mode, measurements can be made over the altitude range between 185 km and 463 km for at least one orbit. Both experiments allow measurements in the altitude range where oxygen is found in both atomic and molecular form and, when applied to atmospheric measurements, will help in the understanding of the physics, chemistry, and dynamics of the upper atmosphere.

Langley Research Center,
National Aeronautics and Space Administration,
Hampton, Va., July 22, 1974.

## REFERENCES


1. Meadows, E. B.; and Townsend, J. W., Jr.: IGY Rocket Measurements of Arctic Atmospheric Composition Above 100 km. Space Research, Hilde Kallman Bijl, ed., Interscience Publ., Inc., 1960, pp. 175-198.

2. Schaefer, E. J.: Composition and Temperature of the Neutral Tropic Lower Thermosphere. J. Geophys. Res., vol. 74, no. 14, July 1969, pp. 3488-3498.

3. Kasprzak, W. T.; Krankowsky, D.; and Nier, Alfred O.: A Study of Day-Night Variations in the Neutral Composition of the Lower Thermosphere. J. Geophys. Res., vol. 73, no. 21, Nov. 1968, pp. 6765-6782.

4. Hedin, A. E.; Avery, C. A.; and Tschetter, C. D.: An Analysis of Spin Modulation Effects on Data Obtained With a Rocket-Borne Mass Spectrometer. J. Geophys. Res., vol. 69, no. 21, Nov. 1964, pp. 4637-4648.

5. Von Zahn, U.: Mass Spectrometric Measurements of Atomic Oxygen in the Upper Atmosphere: A Critical Review. J. Geophys. Res., vol. 72, no. 23, Dec. 1967, pp. 5933-5937.

6. Offermann, D.; and Von Zahn, U.: Atomic Oxygen and Carbon Dioxide in the Lower Thermosphere. J. Geophys. Res., vol. 76, no. 10, Apr. 1971, pp. 2520-2522.

7. Offermann, D.; and Trinkes, H.: A Rocket Borne Mass Spectrometer With Helium Cooled Ion Source. Rev. Sci. Instrum., vol. 42, no. 12, Dec. 1971, pp. 1836-1843.

8. Hedin, A. E.; Hinton, B. B.; and Schmitt, G. A.: Role of Gas-Surface Interactions in the Reduction of OGO 6 Neutral-Particle Mass Spectrometer Data. NASA TN D-7239, 1973.

9. Bleakney, Walker: A New Method of Positive Ray Analysis and Its Application to the Measurement of Ionization Potentials in Mercury Vapor. Phys. Rev., second ser., vol. 34, July-Dec. 1929, pp. 157-160.

10. Nier, Alfred O.: A Mass Spectrometer for Routine Isotope Abundance Measurements. Rev. Sci. Instrum., vol. 11, no. 7, July 1940, pp. 212-216.

11. Callinan, J. P.; and Knuth, E. L.: An Experimental Study of the Particle, Momentum, and Energy Flux Distributions of Products of Collisions of 1 eV Argon Atoms and Surfaces. Rarefied Gas Dynamics, Vol. II, Leon Trilling and Harold Y. Wachman, eds., Academic Press, Inc., 1969, pp. 1247-1255.

12. O'Keefe, D. R.; and French, J. B.: High Energy Scattering of Inert Gases From Well Characterized Surfaces. I – Experimental. Rarefied Gas Dynamics, Vol. II, Leon Trilling and Harold Y. Wachman, eds., Academic Press, Inc., 1969, pp. 1279-1296.

13. Layton, J. K.; Smith, J. N., Jr.; and Saltsburg, H.: Angular Distributions of Fast Scattered Particles Resulting From Collisions of 1- to 60-keV Noble Gases With Metal Surfaces. Rarefied Gas Dynamics, Vol. II, Leon Trilling and Harold Y. Wachman, eds., Academic Press, Inc., 1969, pp. 1297-1302.

14. Palmer, R. L.; Smith, Joe N., Jr.; Saltsburg, Howard; and O'Keefe, D. R.: Measurements of the Reflection, Adsorption, and Desorption of Gases From Smooth Metal Surfaces. J. Chem. Phys., vol. 53, no. 5, Sept. 1, 1970, pp. 1666-1676.

15. Melfi, Leonard Theodore, Jr.: The Design, Development, and Analysis of a Mass Spectrometer System for Number Density Measurements in the Terrestrial Thermosphere. Ph. D. Diss., Florida State Univ., Aug. 1971.

16. Hayward, W. H.; and Jepsen, R. L.: A Simple High Vacuum Gauge Calibration System. 1962 Transactions of the Ninth National Vacuum Symposium of the American Vacuum Society, George H. Bancroft, ed., Macmillan Co., c.1962, pp. 459-462.

17. Melfi, Leonard T., Jr.; and Kern, Frederick A.: Variations in Gage Constant as a Function of Emission Current in an Unshielded Open-End Grid Bayard-Alpert Ionization Gage. NASA TN D-3811, 1967.

18. Simpson, J. Arol: Design of Retarding Field Energy Analyzers. Rev. Sci. Instrum., vol. 32, no. 12, Dec. 1961, pp. 1283-1293.

19. Jacchia, L. G.: New Static Models of the Thermosphere and Exosphere With Empirical Temperature Profiles. Spec. Rep. No. 313, Smithsonian Astrophys. Observ., May 6, 1970. (Available as NASA CR-112684.)

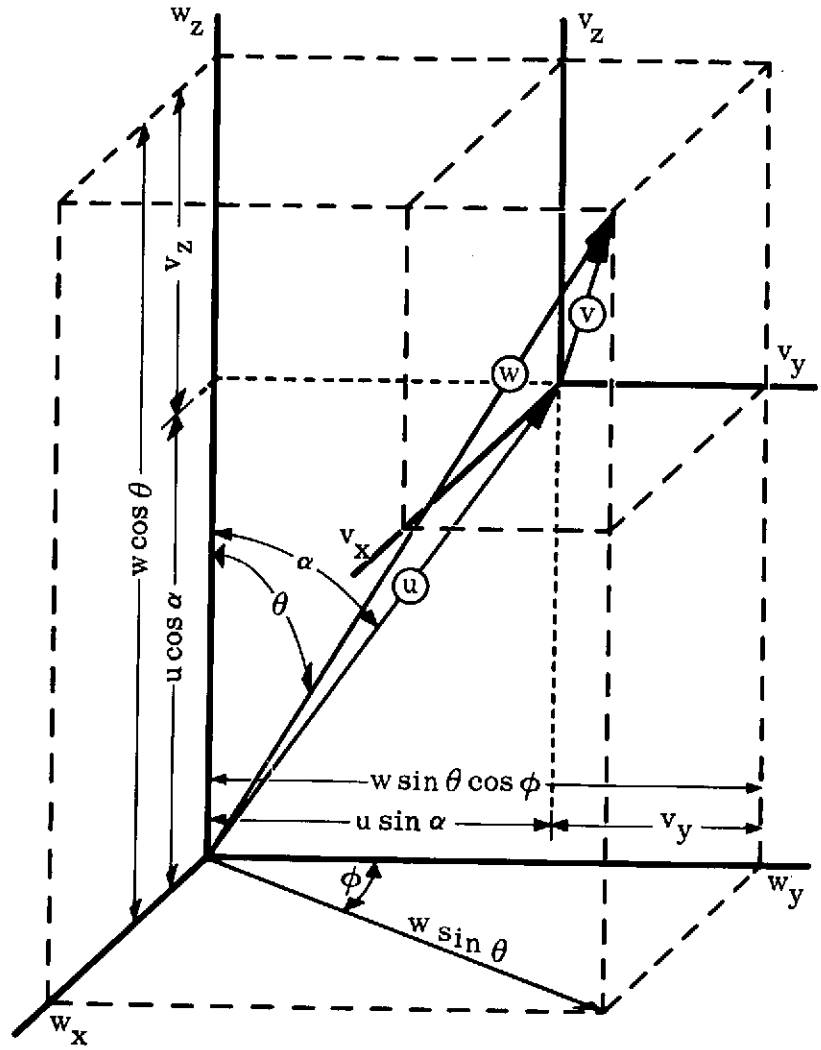


Figure 1.- Velocity-space coordinate system for transformation to drifting spherical coordinates $w, \theta, \phi$.

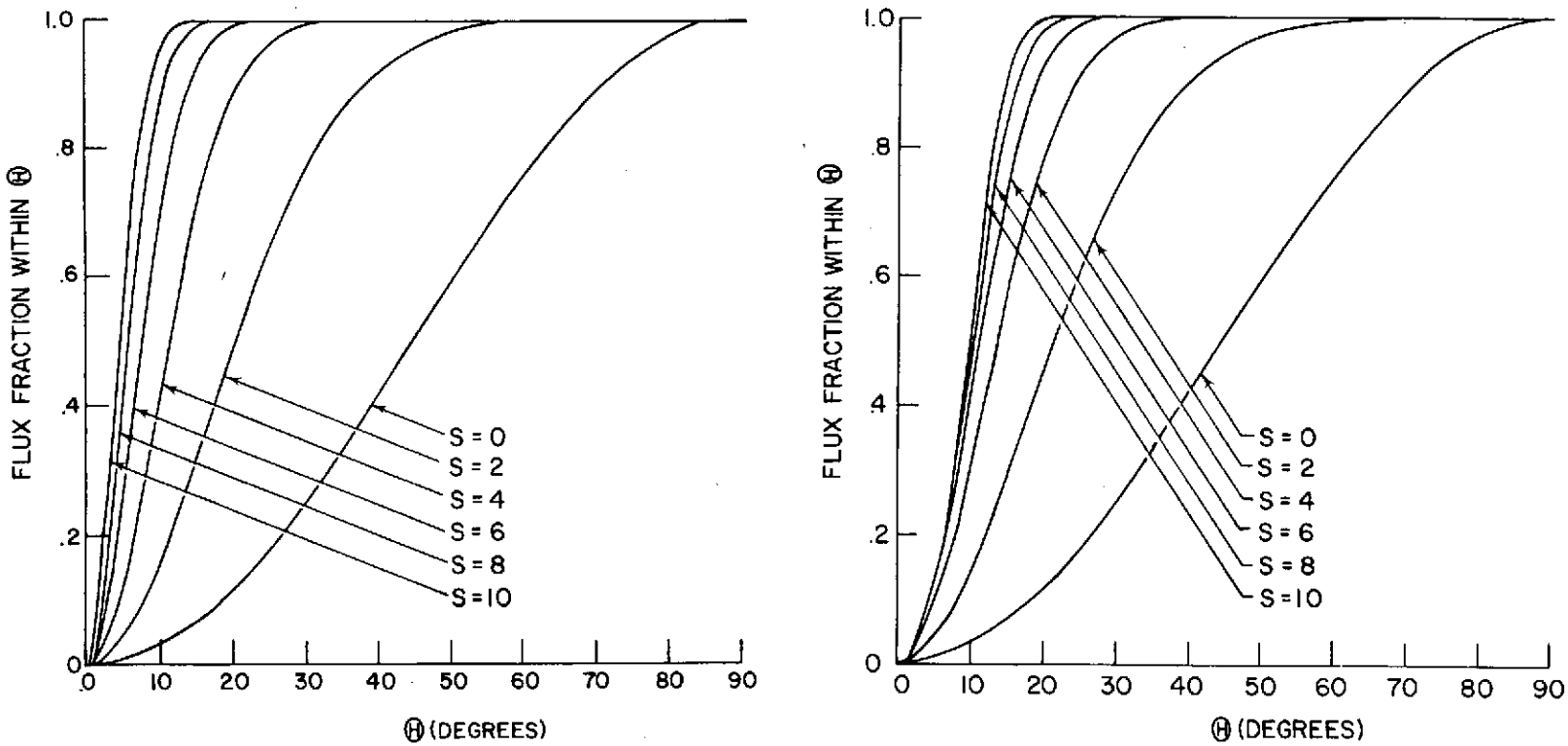


(a) $\alpha = 0^{o}$.

(b) $\alpha = 9^{o}$.

Figure 2.- Calculated value of flux $\left[F(S,\alpha,\Theta)/F(S,\alpha,\pi/2)\right]$ from equations (2) and (4) through an incremental surface for the solid angle $\Theta$ in front of the surface at different speed ratios S (eq. (3)).

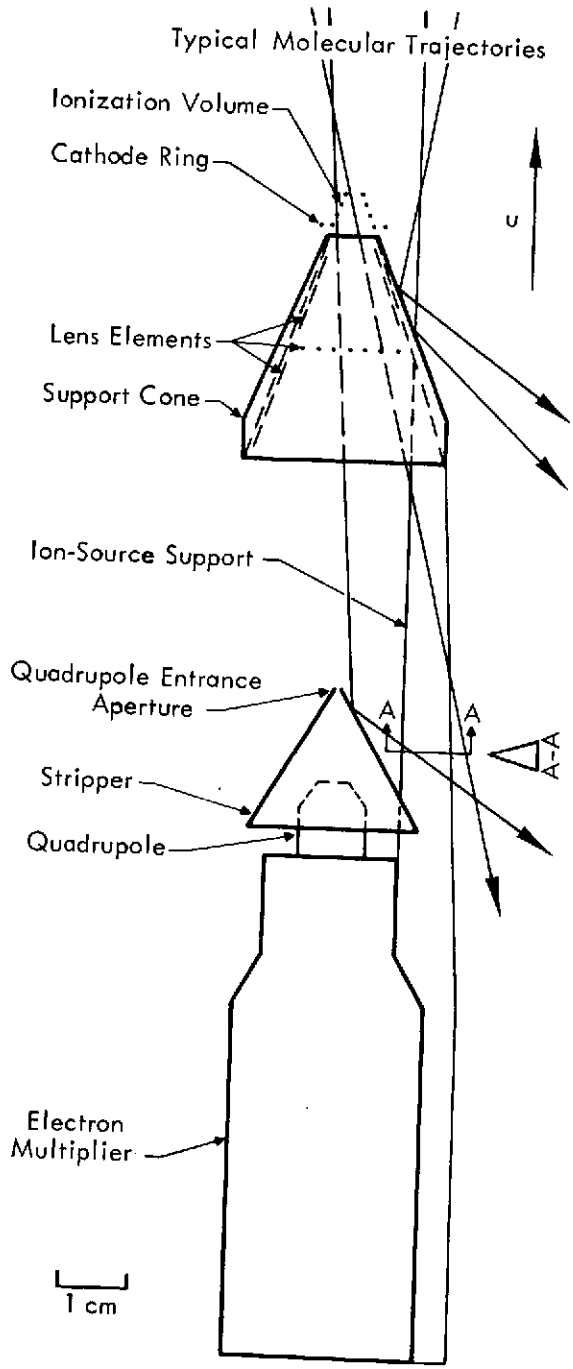


Figure 3.- Molecular beam mass spectrometer.

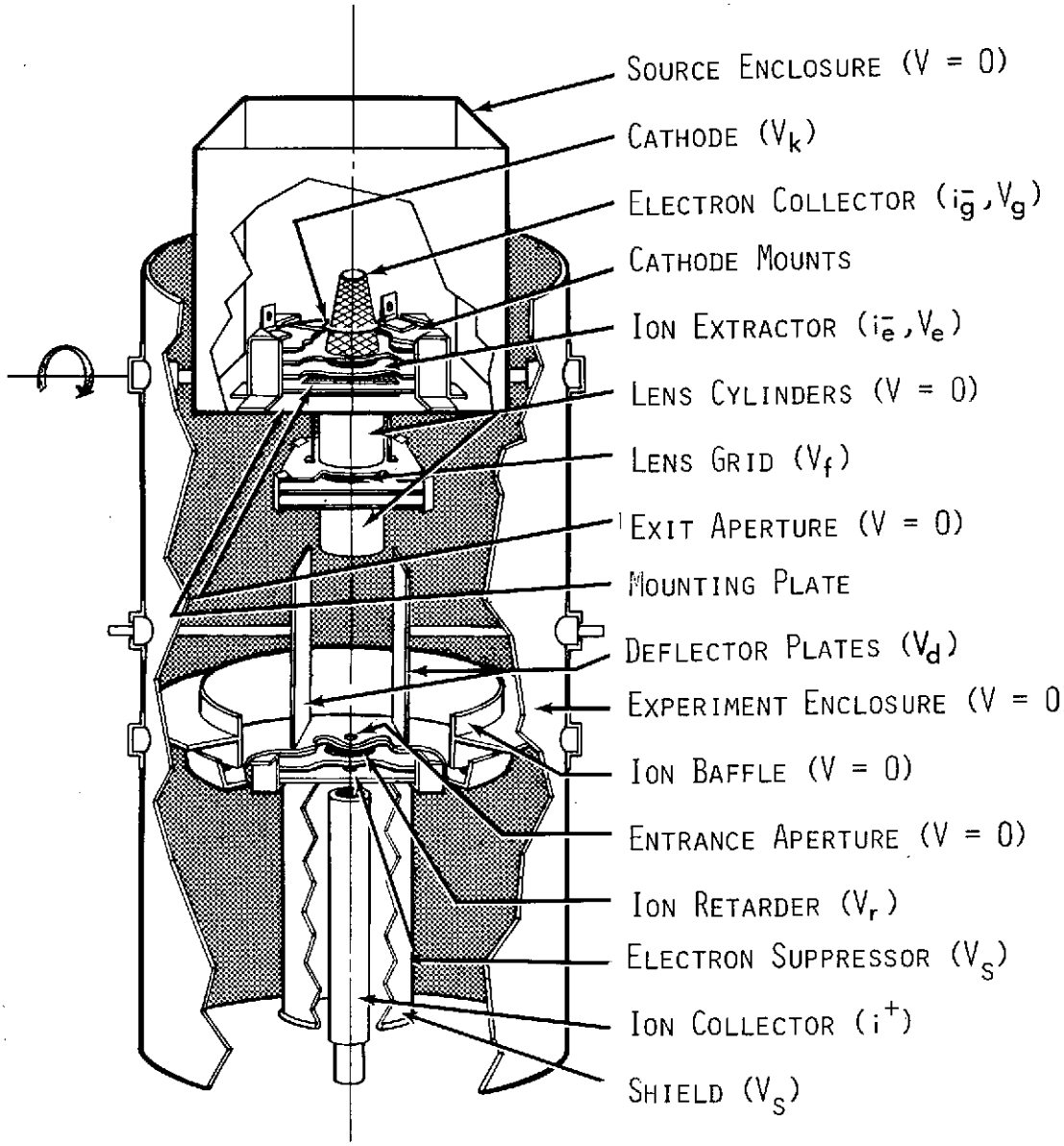


Figure 4.- Ion-beam analysis apparatus used to evaluate the energy distributions and angular distributions of the ion beam extracted from the transparent free-stream ion source.

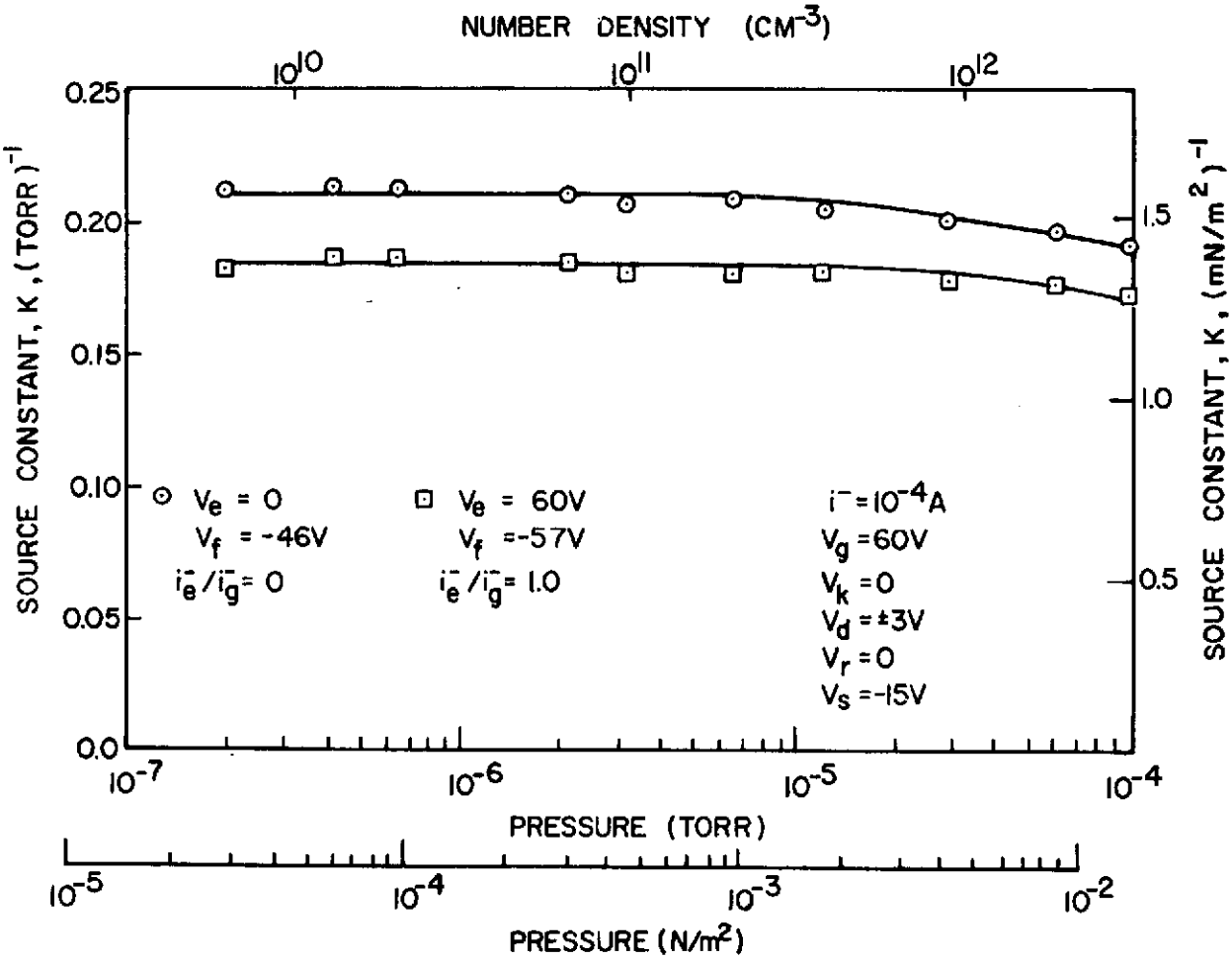


Figure 5.- Source constant (eq. (5)) as a function of pressure for two source electrical configurations.

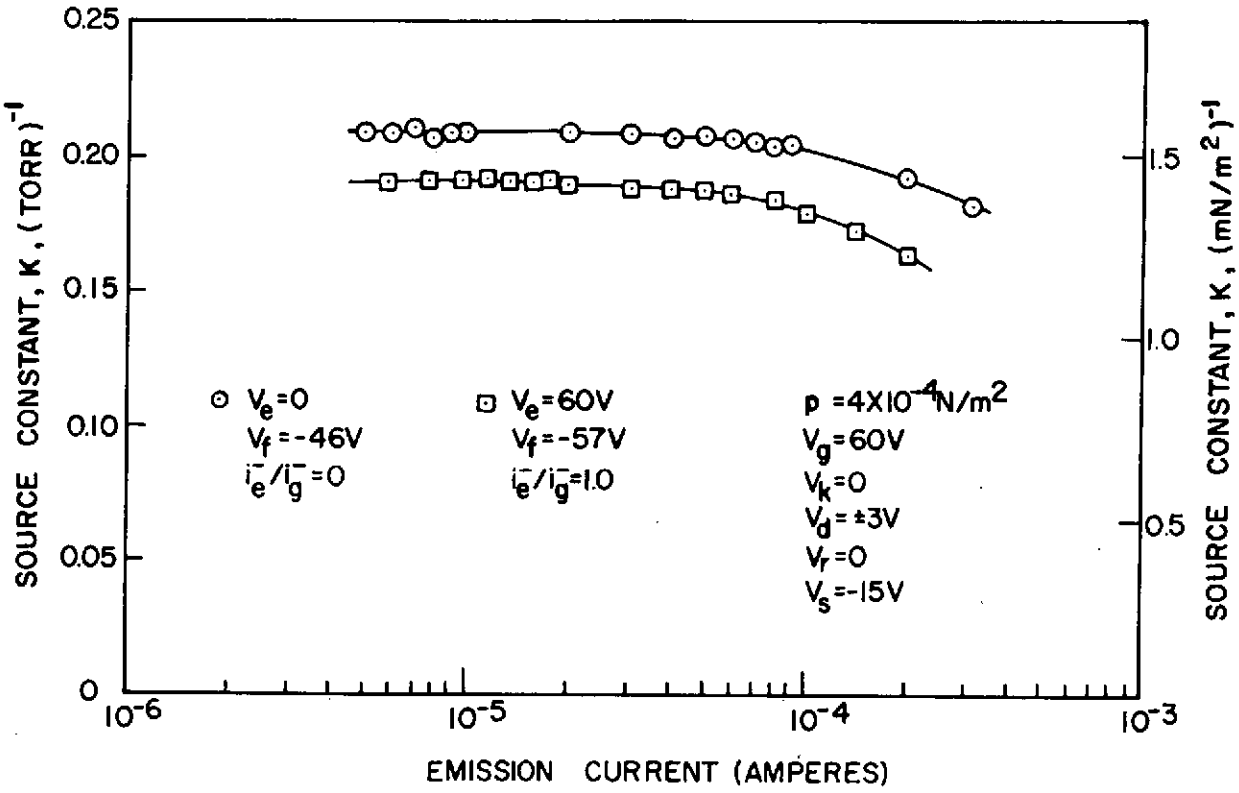


Figure 6. - Source constant (eq. (5)) as a function of emission current for two source electrical configurations. (The emission current is defined as the sum of the electron currents collected at the grid $i_g^-$ and at the extractor $i_e^-$.)

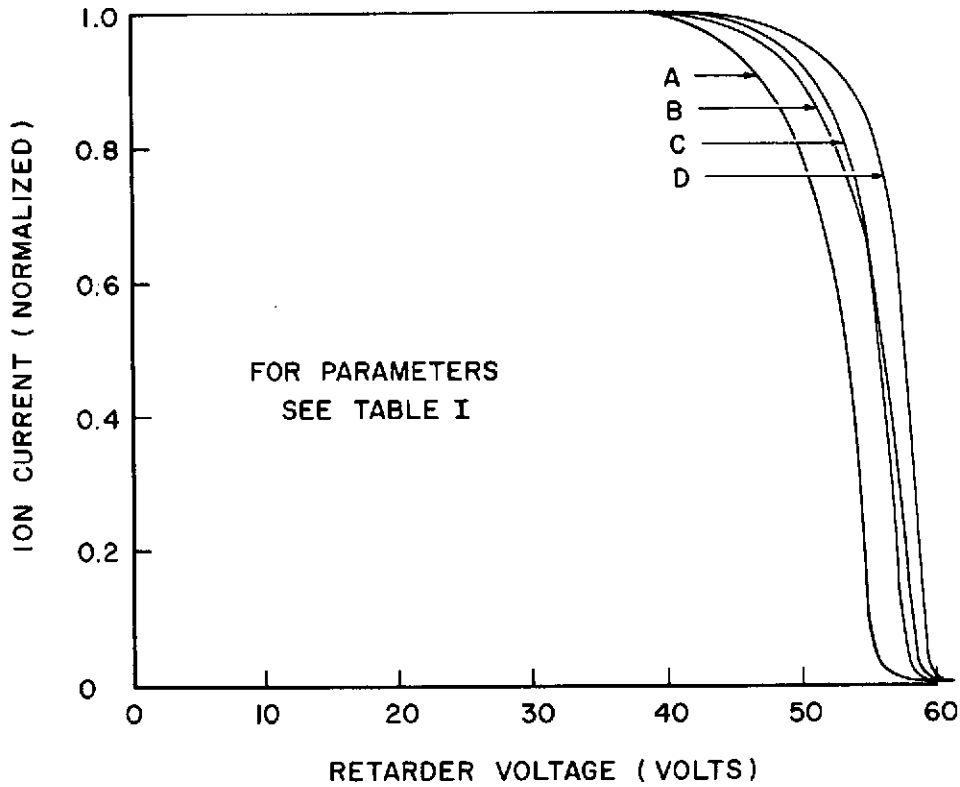


Figure 7.- Normalized ion current at the Faraday collector as a function of retarder potential for a number of source electrical configurations.

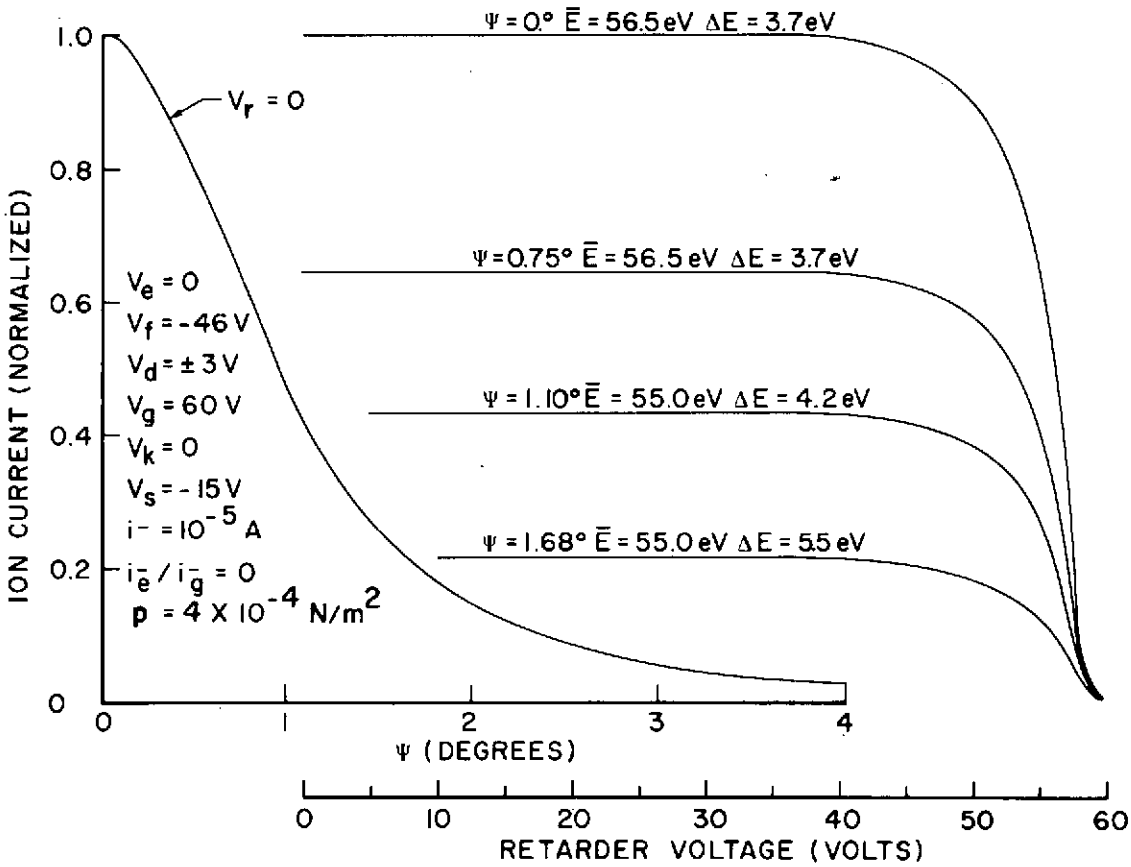


(a) Extractor voltage, $V_e = 0$.

Figure 8.- Normalized ion current as a function of angular displacement $\Psi$ of the ion beam (left side) and as a function of retarder voltage for a number of values of $\Psi$ (right side).

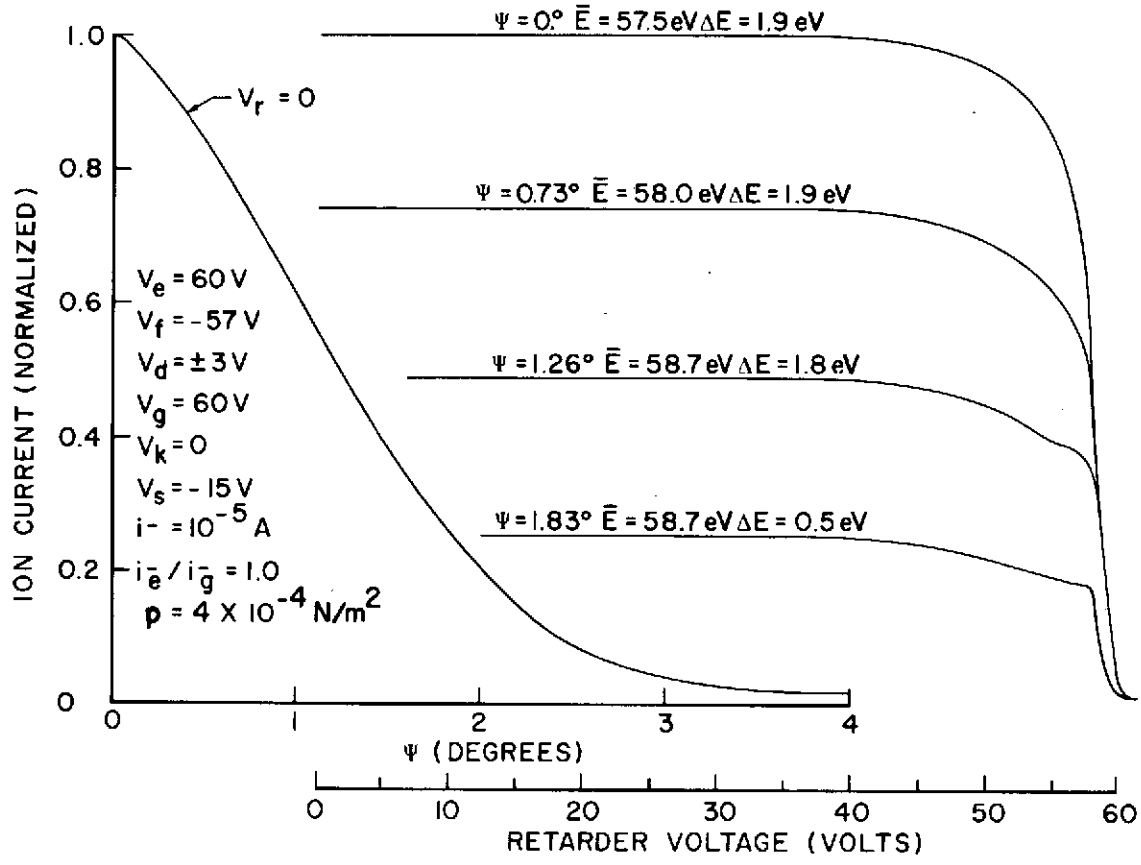


(b) Extractor voltage, $V_e$ = 60 V.

Figure 8.- Concluded.

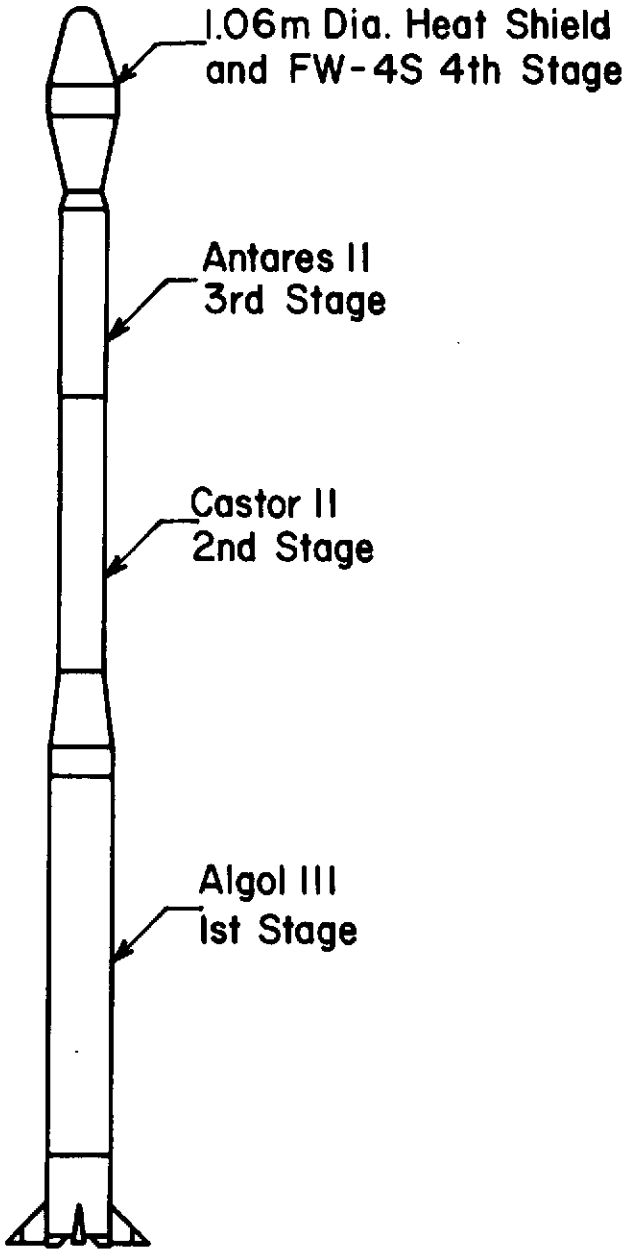


(a) Scout vehicle.

Figure 9.- Scout vehicle, third stage of Scout vehicle showing possible mass spectrometer location, and trajectory of third stage.

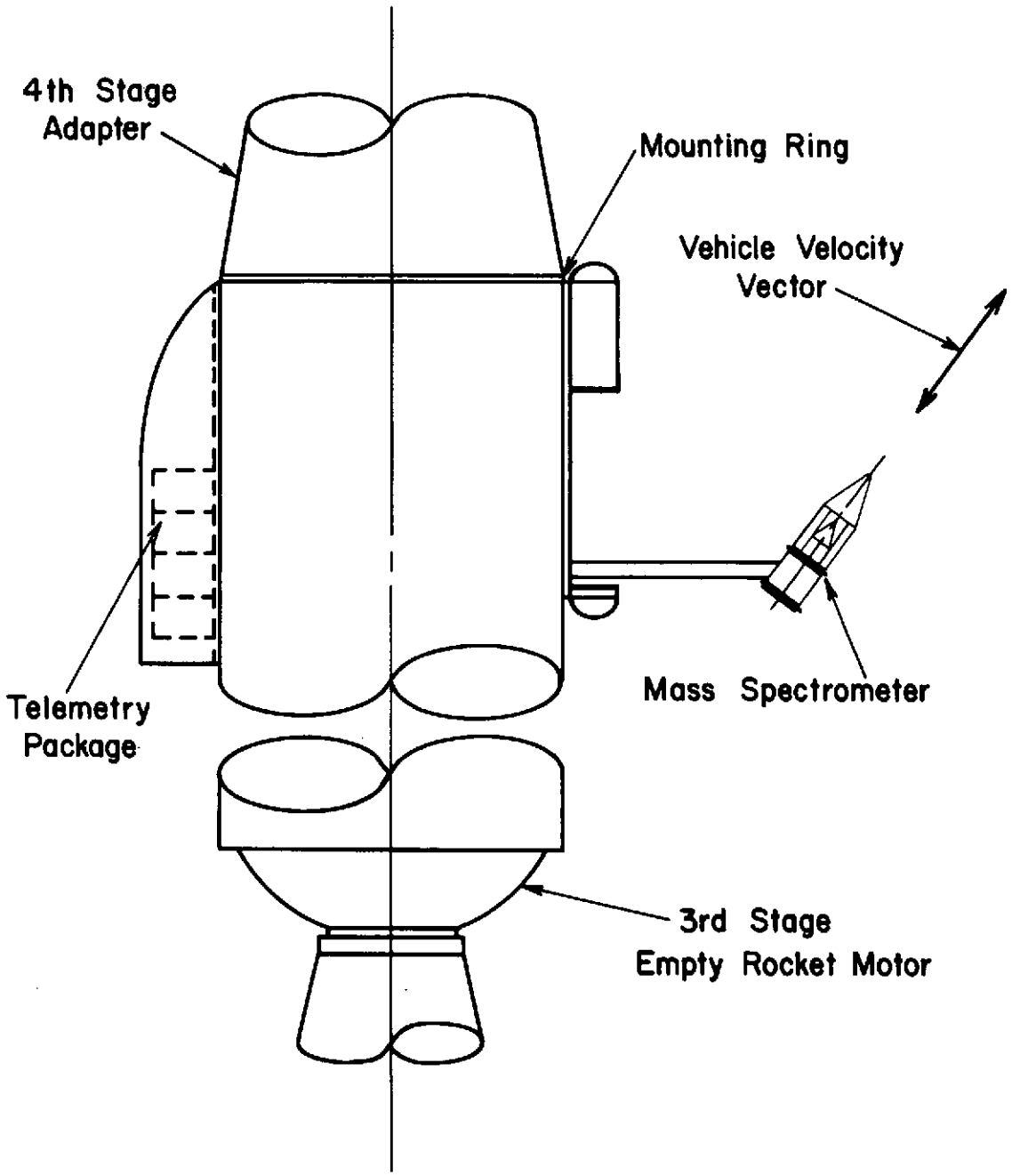


(b) Third stage (Antares II rocket motor) of Scout vehicle with mass spectrometer deployed.

Figure 9.- Continued.

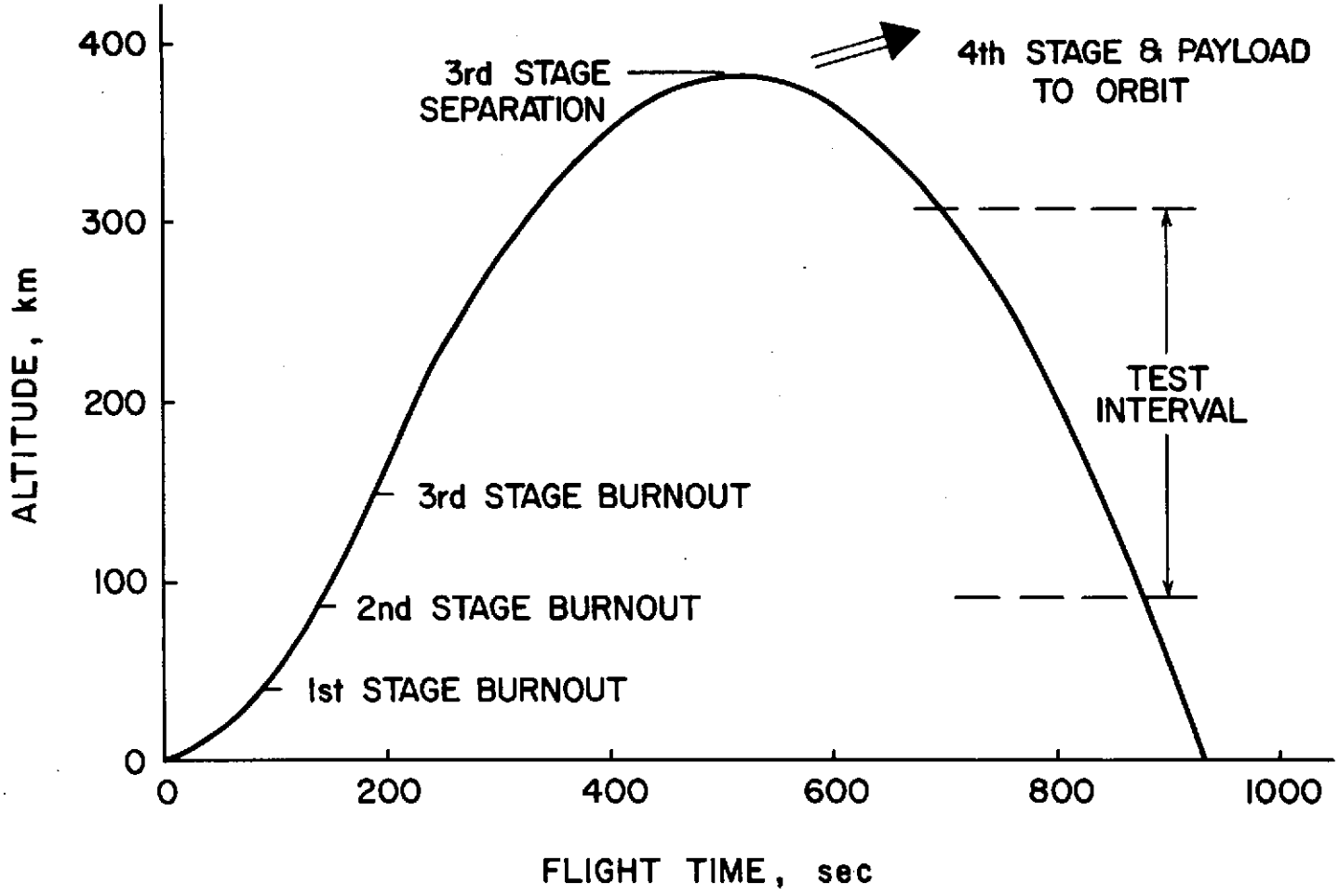


(c) Trajectory of third stage and test interval.

Figure 9.- Concluded.

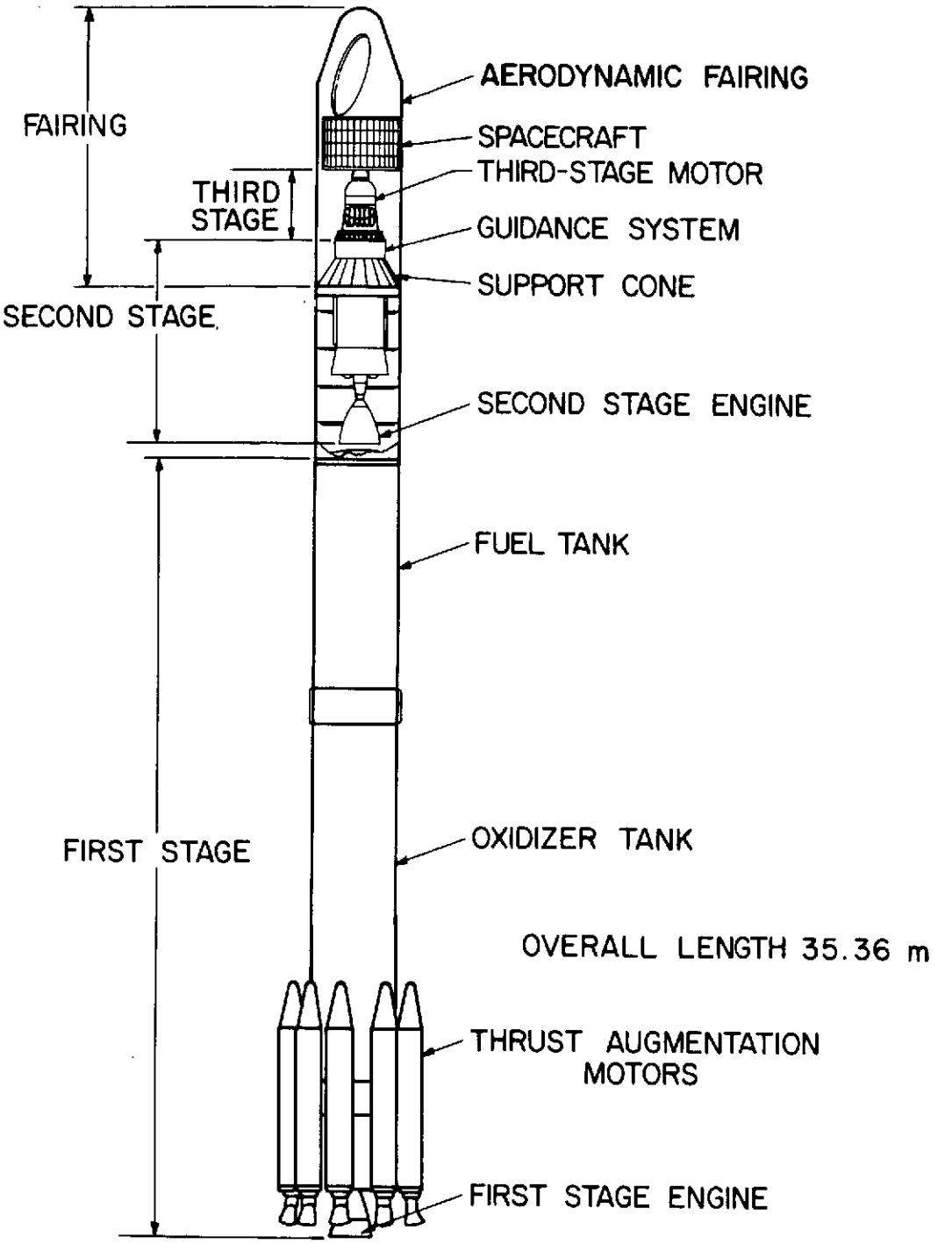


(a) Delta vehicle.

Figure 10.- Delta vehicle, location of mass spectrometer mounted on Delta second stage (stored and deployed), and ground track of Delta orbit.

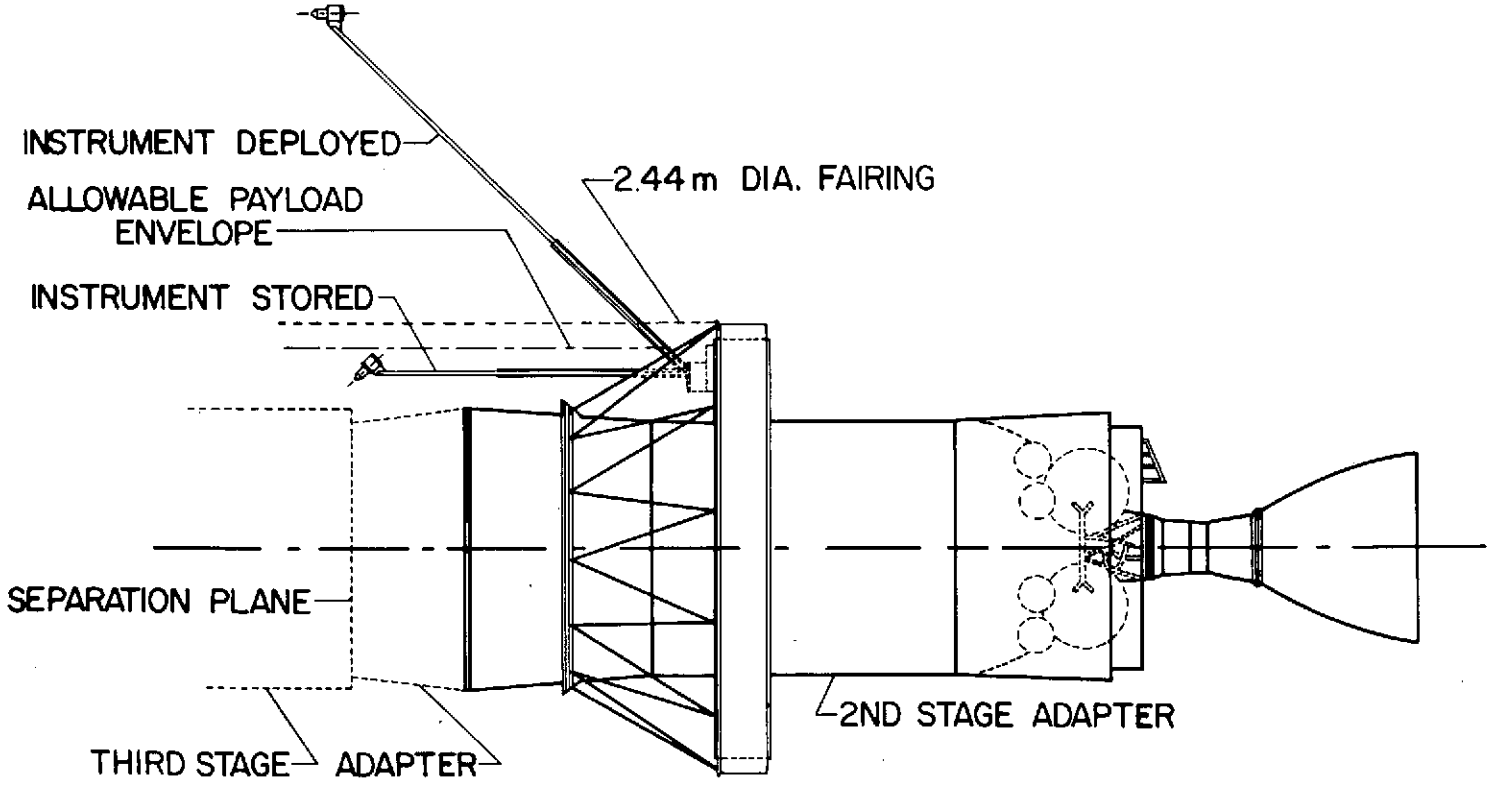


(b) Mass spectrometer (stored and deployed) on second stage of Delta vehicle.

Figure 10.- Continued.

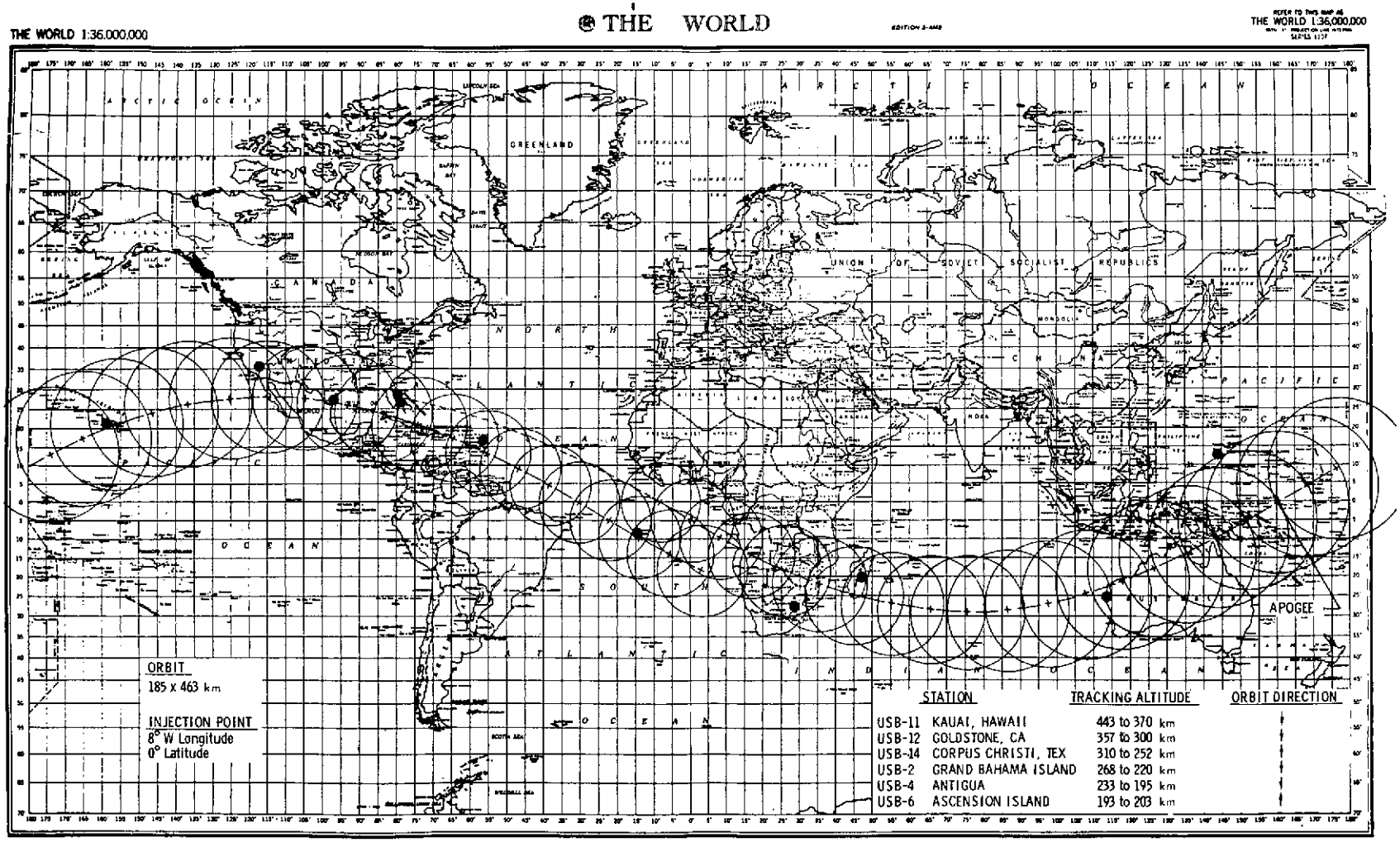


(c) Ground track of second stage of Delta vehicle with tracking stations and altitude of orbit at each station.

Figure 10.- Concluded.